A crystallographic analysis of the macrodomain structure in $Pb(Mg_{1/3}Nb_{2/3})O_3$

Topolov, V.Yu.; Ye, Zuo-Guang; Schmid, Hans

J. Phys.: Condens. Matter 7 (1995) 3041–3049. Printed in the UK

A crystallographic analysis of the macrodomain structure in $Pb(Mg_{1/3}Nb_{2/3})O_3$

V Yu Topolov†, Z-G Ye‡ and H Schmid‡

† Physics Faculty, Rostov State University, 344104 Rostov-on-Don, Russia

‡ Department of Mineral, Analytical and Applied Chemistry, University of Geneva, CH-1211 Geneva 4, Switzerland

Received 10 November 1994

Abstract. A crystallographic analysis of the ferroelectric/ferroelastic domains and phase boundaries in thin platelets of $Pb(Mg_{1/3}Nb_{2/3})O_3$, associated with the electric-field-induced phase transition from the disordered cubic phase to the induced $3m$ phase, is reported. Calculations have been performed by taking into account the internal stresses and their relation to the unit cell parameters. The results have permitted us to interpret the experimentally observed polar macrodomain structure, phase boundary and switching of the induced polarization. A diagram connecting the possible domain types and the shapes of the $m\bar{3}m \leftrightarrows 3m$ phase boundaries has been proposed. The role of the several domain types and features of their elastic matching have also been analysed.

1. Introduction

The complex perovskite $Pb(Mg_{1/3}Nb_{2/3})O_3$ (PMN) is known to show a typical dielectric relaxor behaviour with the broad maximum of the dielectric permittivity ($> 10^4$ at 1 kHz) near 265 K; the temperature depends upon the frequency of the exciting electric field [1]. This maximum of the dielectric constant was considered to result from a 'diffuse ferroelectric phase transition' phenomenon due to the disordered cations in B site (B′;B″) and the composition fluctuations [2]. Macroscopically no evidence indicating a phase transition into a ferroelectric phase can be obtained at zero electric field, the PMN crystals remaining optically isotropic to longer-coherent-length-probing radiations, such as polarized light or x-rays. No optical macrodomains can therefore be observed, although the presence of the chemically inhomogeneous polar nanodomains was revealed both by high-resolution electron microscopy [3] and by diffuse scattering of the x-ray and neutron diffraction lines [4]. Evidence for a first-order electric-field-induced phase transition in PMN crystals, from the disordered cubic phase to a polar trigonal $3m$ phase, has recently been disclosed by studying the dielectric anomalies, the establishment of the induced polarization, the onset of the poling current and especially the appearance of the optical polar macrodomains and phase boundaries during the induced phase transition [5, 6].

It is well known that the formation of domains in the ferroelectric, ferroelastic and related materials are closely associated with the energetics of the ferroic phase transitions [7, 8]. However, it is in general a very difficult problem to determine the domain structure parameters by minimization of the free energy containing different contributions. In the previous papers much attention was given to the study of the elastic interactions in ferroelastic [9], ferroelectric [10–12] and antiferroelectric [13, 14] polydomain crystals. A crystallographic description of the interacting domains or phases on the basis of Metrat's

0953-8984/95/153041+09$19.50

theory [10] has been shown to be effective for prediction of the equilibrium domain structures and phase boundaries, being the zero-net-strain (stress-free) planes [15, 16]. The purpose of the present work was to study the domain structure and phase boundary related to the electric-field-induced $m\bar{3}m \rightarrow 3m$ phase transition in thin PMN crystal samples, by means of the crystallographic method developed previously.

2. Macrodomain structure and the phase boundary

The electric-field-induced phase transition in PMN has been evidenced, among other ways, by the appearance below the transition temperature of the birefringent macrodomains on $(100)_{cub}$ and $(110)_{cub}$ platelets with the electric field strength vector $\boldsymbol{E}$ parallel to $\langle 100\rangle_{cub}$ and $\langle 110\rangle_{cub}$ directions, respectively (see figure 7 in [5] and figure 5 in [6]). On a $(111)_{cub}$ plane, however, the induced phase transition was revealed by the onset of a phase boundary (at 230 K for $\boldsymbol{E}_{\|}\langle 111\rangle_{cub} = 3$ kV cm^{-1}), separating the cubic phase and the field-induced polar $3m$ phase, indicating a first-order electric-field-induced phase transition. During the establishment of the induced phase, the phase boundary travelled through the crystal while the induced phase gained the area of the disappearing cubic phase, leading to a homogeneous monodomain state at the end of the phase transition. This induced trigonal phase behaved optically isotropically when observed along $\langle 111\rangle_{cub} \| \boldsymbol{E}_{poling}$. The sequence of such an induced phase transition is illustrated in figure 1 (see also figure 8 in [5] and figure 3 in [6]).

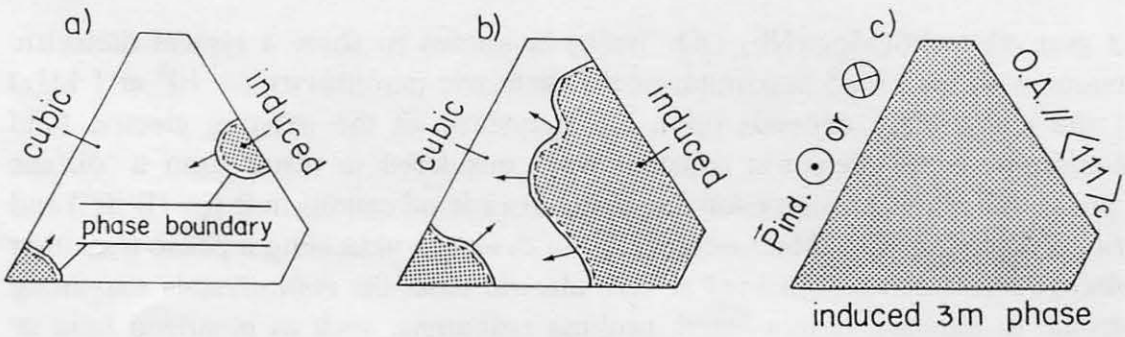

Figure 1. A schematic representation of the sequence of the electric-field-induced $m\bar{3}m \rightarrow 3m$ phase transition observed on a $(111)_{cub}$ platelet of PMN ($\boldsymbol{E}_{\|\langle 111\rangle cub} = 3$ kV cm^{-1}) near 230 K by means of polarized light microscopy: (a) the onset of the phase induction shown up by the appearance of the phase boundary delimiting the induced phase and the mean cubic phase; (b) the propagation of the phase boundary through the crystal plate with the growth of the induced phase; (c) the monodomain state of the induced $3m$ phase behaving isotropically along $\langle 111\rangle_{cub}$.

Once the macropolarization has been induced, it remains metastable and can be switched by an electric field of opposite polarity ($E = \pm 3$ kV cm^{-1}, $T = 175$–200 K), showing the ferroelectric properties. Optical domain observations showed that the 180° switching process of the induced polarization takes place via intermediate ferroelastic orientation states of the $3m$ phase with their optical axis and polarization vector inclined by about 35° to the $(111)_{cub}$ plane, giving rise to the birefringent lamellar domains. These lamellar domains transformed thereafter into an isotropic section but with the induced polarization $\boldsymbol{P}_{ind}$ reversed by 180° (see figure 16 in [5] and figures 6–8 in [6]).

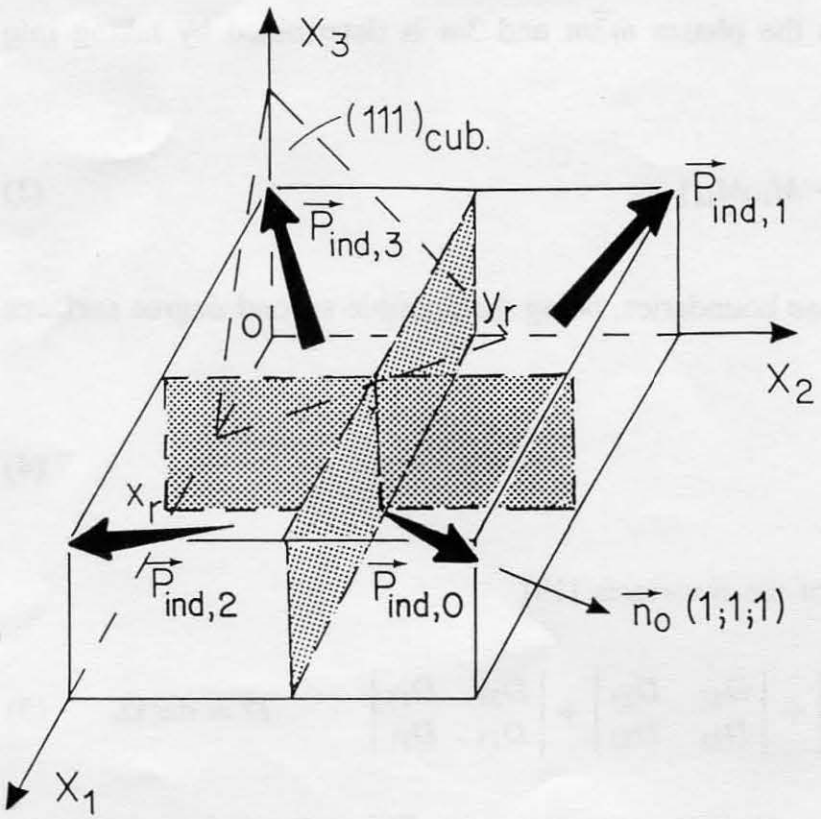

Figure 2. A scheme of the possible non-180° domain types (i.e. the mechanical twin components) in the $3m$ phase of PMN crystals. $\boldsymbol{P}_{\mathrm{ind},l}$ ($l = 0; 1; 2; 3$) are the induced polarization vectors shown by the bold arrows. The $(111)_{\mathrm{cub}}$ plane and its normal vector $\boldsymbol{n}_0$ are also indicated.

3. An analysis of domain structure and the phase boundary

Some features of the electric-field-induced $m\bar{3}m \rightarrow 3m$ phase transition in PMN platelets can be analysed by using the crystallographic method developed in [17] and [18]. The four possible types of non-180° domain ($l = 0; 1; 2; 3$) in the induced $3m$ phase, as shown in figure 2, are characterized by the field-induced polarization vectors $\boldsymbol{P}_{\mathrm{ind},0}(P; P; P)$, $\boldsymbol{P}_{\mathrm{ind},1}(-P; P; P)$, $\boldsymbol{P}_{\mathrm{ind},2}(P; -P; P)$ and $\boldsymbol{P}_{\mathrm{ind},3}(-P; -P; P)$ as well as by the volume concentrations

$$o_0 = (1 - x_\mathrm{r})(1 - y_\mathrm{r}) \qquad o_1 = x_\mathrm{r}(1 - y_\mathrm{r}) \qquad o_2 = (1 - x_\mathrm{r})y_\mathrm{r} \qquad o_3 = x_\mathrm{r}y_\mathrm{r} \tag{1}$$

respectively, where x_r and y_r are the parameters representing the relative width of the domains. The distortion matrices $\mathbf{N}_i$ of the domain types mentioned above can be written in the Cartesian system $(X_1X_2X_3)$ as

$$\mathbf{N}_0 = \begin{pmatrix} \eta_\mathrm{a} & \eta & \eta \\ \eta & \eta_\mathrm{a} & \eta \\ \eta & \eta & \eta_\mathrm{a} \end{pmatrix} \qquad \mathbf{N}_1 = \begin{pmatrix} \eta_\mathrm{a} & -\eta & -\eta \\ -\eta & \eta_\mathrm{a} & \eta \\ -\eta & \eta & \eta_\mathrm{a} \end{pmatrix}$$
$$\mathbf{N}_2 = \begin{pmatrix} \eta_\mathrm{a} & -\eta & \eta \\ -\eta & \eta_\mathrm{a} & -\eta \\ \eta & -\eta & \eta_\mathrm{a} \end{pmatrix} \qquad \mathbf{N}_3 = \begin{pmatrix} \eta_\mathrm{a} & \eta & -\eta \\ \eta & \eta_\mathrm{a} & -\eta \\ -\eta & -\eta & \eta_\mathrm{a} \end{pmatrix} \tag{2}$$

where $\eta_\mathrm{a} = a_\mathrm{rh} \cos \omega/a_\mathrm{c}$ and $\eta = a_\mathrm{rh} \sin \omega/a_\mathrm{c}$ are the unit cell distortions expressed by the unit cell dimensions a_rh (rhombohedral $3m$ phase), a_c (cubic $m\bar{3}m$ phase) and the shear angle ω (phase $3m$) in the cubic axes. The matrix $\mathbf{M}$ of the initial unstrained $m\bar{3}m$ phase is determined by the Kronecker symbol $M_{ij} = \delta_{ij}$ as a unit matrix. All the elements of the matrix $\mathbf{N}$ of the polydomain $3m$ phase are given in the form of

$$N_{ij} = \sum_{l=0}^{3} o_l N_{l,ij}$$

where o_l and $N_{l,ij}$ are taken from equations (1) and (2), respectively.

An elastic interaction between the phases $m\bar{3}m$ and $3m$ is determined by taking into account the elements [10, 17, 18]

$$D_{ij} = \sum_{k=1}^{3} (N_{ik}N_{jk} - M_{ik}M_{jk}) \tag{3}$$

which have an influence on the phase boundaries, being the possible second-degree surfaces [17, 18]

$$\sum_{i,j=1}^{3} D_{ij}x_i x_j = 0. \tag{4}$$

Their shapes depend on the signs of the invariants [19]

$$I = \sum_{i=1}^{3} D_{ii} \qquad J = \begin{vmatrix} D_{11} & D_{12} \\ D_{12} & D_{22} \end{vmatrix} + \begin{vmatrix} D_{22} & D_{23} \\ D_{23} & D_{33} \end{vmatrix} + \begin{vmatrix} D_{33} & D_{13} \\ D_{13} & D_{11} \end{vmatrix} \qquad D = \det \mathbf{D}. \tag{5}$$

The central place among the surfaces (4) belongs to the cones. This type of phase boundary has been analysed in the case of their visualization on $(100)_{cub}$ platelets of perovskite polydomain single crystals [17, 18]. In the present work, the possible phase boundaries occurring on the $(111)_{cub}$ PMN platelet are studied. For this purpose, we have carried out a transformation of the coordinate axes $(X_1X_2X_3) \rightarrow (X_1'X_2'X_3')$ by a rotation of $(OX_1) \rightarrow (OX_1')$ at an angle of 45° and $(OX_3) \rightarrow (OX_3')$ at such an angle that the direction of the (OX_3') axis coincides with the $\boldsymbol{n}_0$ (1; 1; 1) vector, as shown in figure 2. This transformation is written in the form of

$$x_1 = \tfrac{1}{2}\left(x_1' - x_2' + \sqrt{2}x_3'\right) \qquad x_2 = \left(\sqrt{2}/2\right)(x_1' + x_2') \qquad x_3 = \tfrac{1}{2}\left(-x_1' + x_2' + \sqrt{2}x_3'\right). \tag{6}$$

The subsequent substitution of equations (6) into equation (4) leads to a new equation:

$$\tilde{D}_{11}x_1'^2 + \tilde{D}_{22}x_2'^2 + \tilde{D}_{33}x_3'^2 + 2\tilde{D}_{12}x_1'x_2' + 2\tilde{D}_{13}x_1'x_3' + 2\tilde{D}_{23}x_2'x_3' = 0 \tag{7}$$

where

$$\tilde{D}_{11} = \tfrac{1}{4}(D_{11} + D_{33}) + \tfrac{1}{2}(D_{22} - D_{13}) + \left(\sqrt{2}/2\right)(D_{12} - D_{23})$$

$$\tilde{D}_{22} = \tfrac{1}{4}(D_{11} + D_{33}) + \tfrac{1}{2}(D_{22} - D_{13}) - \left(\sqrt{2}/2\right)(D_{12} - D_{23})$$

$$\tilde{D}_{33} = \tfrac{1}{2}(D_{11} + D_{33}) + D_{13}$$

$$\tilde{D}_{12} = -\tfrac{1}{4}(D_{11} + D_{33}) + \tfrac{1}{2}(D_{13} + D_{22})$$

$$\tilde{D}_{13} = \tfrac{1}{2}(D_{12} + D_{23}) - \left(\sqrt{2}/4\right)(D_{33} - D_{11})$$

$$\tilde{D}_{23} = \tfrac{1}{2}(D_{12} + D_{23}) + \left(\sqrt{2}/4\right)(D_{33} - D_{11}).$$

Consideration of a phase boundary section by a plane $x = f$ with $f = \text{constant} \neq 0$, i.e. by the $(111)_{cub}$ plane, is realized by the further transformation of equation (7) with control of the signs of the invariants [19]:

$$I_0 = \tilde{D}_{11} + \tilde{D}_{22} \qquad D_0 = \begin{vmatrix} \tilde{D}_{11} & \tilde{D}_{12} \\ \tilde{D}_{12} & \tilde{D}_{22} \end{vmatrix} \qquad A_0 = \begin{vmatrix} \tilde{D}_{11} & \tilde{D}_{12} & \tilde{D}_{13}f \\ \tilde{D}_{12} & \tilde{D}_{22} & \tilde{D}_{23}f \\ \tilde{D}_{13}f & \tilde{D}_{23}f & \tilde{D}_{33}f \end{vmatrix} = f^2 \det \mathbf{D} \tag{8}$$

which are related to a second-degree curve.

Our calculations have been carried out by using the unit cell parameters of PMN [20, 21] measured on ceramic and crystal samples within the phase transition region ($a_{rh} = 4.0400$ Å, $\omega = 0.07°$ and $a_c = 4.0441$ Å). A diagram connecting the possible domain types and the shapes of the $m\bar{3}m \leftrightarrows 3m$ phase boundaries shows a lack of unstrained planes for such a phase matching and a sufficiently vast region related to the conic surfaces (figure 3). An interesting feature of these conic phase boundaries can be considered as follows. For all the parameters $(x_r; y_r)$ in the regions I and II (figure 3) one can evaluate the determinant D from equations (5), which characterizes the strains at the phase boundaries. Different evaluations show that, in the case of PMN, as a rule, $|D| \approx 10^{-10}$–10^{-8}, whereas, on average, $|D_{ij}| \approx 10^{-3}$. This circumstance may be the reason for the small mechanical stress arising at the phase boundaries and for a certain unsteadiness leading to their ephemeral appearance, to the different fragments of several conic phase boundaries and to the visible changes in the domain structure (see figure 1).

An important fragment of the diagram ($x_r \to 0$, $y_r \to 0$ in figure 3) corresponds to the central role of the domain type with $P_{ind,0} \perp (111)_{cub}$. The phase transition $m\bar{3}m \to 3m$ in PMN crystals is realized by the formation of this type of domain (single-domain state) or of the types of domain corresponding to the vast regions I and II.

As defined from the invariants (8) in the regions I and II, the possible phase boundary sections on the $(111)_{cub}$ plane of a platelike crystal of PMN are ellipses. To conceive a diversity of allowed ellipse orientations we introduce an angle of rotation of the ellipse axes OX_i^{el} in the $(X_1'OX_2')$ plane

$$\alpha_{el} = \tfrac{1}{2} \tan^{-1}[2\tilde{D}_{12}/(\tilde{D}_{11} - \tilde{D}_{22})] \tag{9}$$

where D_{ij} are as used in equation (7). The results of the calculation are shown in figure 4. The negative sign of all values corresponds to the clockwise rotation of the axes $(OX_1') \to (OX_1^{el})$. Such a diversity of orientations of the possible sections on the $(111)_{cub}$ plane testifies also to the plurality of the phase boundaries and domain structures observable at the induced phase transition in PMN crystals [5, 6].

A comparison of the diagram for the $m\bar{3}m \leftrightarrows 3m$ phase transition in PMN crystals (figure 3) with an analogous known diagram for the first-order ferroelectric phase transition in $PbZrO_3$ crystals [17] allows us to ascertain that the presence of three vast regions belonging to the conic surfaces and the existence of the unusual curve corresponding to the zero-net-strain planes are characteristic of $PbZrO_3$ crystals. A certain shift of the curves in the diagram by consideration of PMN crystals may be associated with a change in the structural parameters [17, 20–22] and with the unit cell spontaneous strains, $\xi_a^s = \eta_a - 1$ and $\xi^s = \eta$, of these crystals at the phase transitions ($\xi_a^s/\xi^s = -0.832$ for PMN and $\xi_a^s/\xi^s = 0.523$ for $PbZrO_3$), which have significant influence on the elements D_{ij} of equation (3) and on the invariants of equations (5).

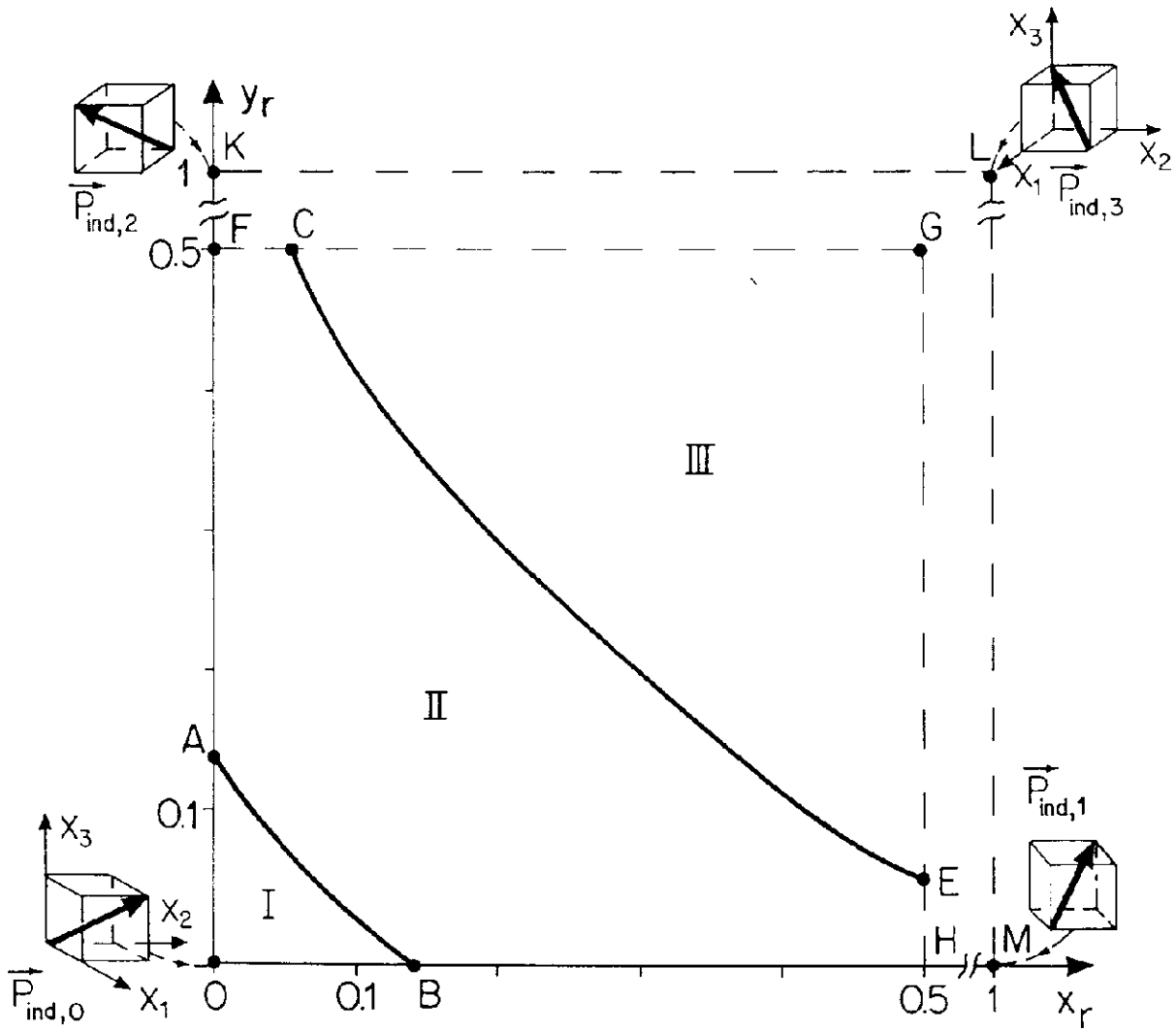

Figure 3. A diagram describing the domain types and phase boundaries determined for the $m\bar{3}m \leftrightarrows 3m$ phase transition in PMN crystals. Regions I ($DI < 0$, $J < 0$) and II ($DI < 0$, $J > 0$) correspond to the conic shapes of the phase boundaries; region III ($DI > 0$, $j > 0$) corresponds to the vertex of the imaginary cone; curves AB and CE correspond to the conditions $J = 0$ and $D = 0$, respectively. Regions $0.5 \leqslant x_r \leqslant 1$, $0.5 \leqslant y_r \leqslant 1$ are generated by transformation of the square OFGH relative to the symmetry axes FG ($y_r = 0.5$) and GH ($x_r = 0.5$). Points O, K, L and M correspond to the single-domain states of the $3m$ phase. All the invariants D, I and J were taken from equations (5).

4. An analysis of domain switching

To date one can give an example of a short crystallographic study of the domain (twin) structure in the $3m$ phase of platelike $PbZrO_3$ crystals only [16, 22]. The formation and rearrangement of the domains during the induced and/or the diffuse phase transitions in the relaxor ferroelectric crystals have not yet been studied by crystallographic methods. This paragraph is therefore devoted to the analogous problem related to the electric-field-induced $m\bar{3}m \rightarrow 3m$ phase transition in platelike PMN single crystals, with the switching of the induced polarization [5, 6].

We have proposed above that the four types of non-180° domain (i.e. mechanical twins) can arise during the $m\bar{3}m \rightarrow 3m$ phase transition (figure 2). A lateral section of the crystal platelet with the domains having the induced polarization vectors $\boldsymbol{P}_{ind,0}$ (the initial domain), $\boldsymbol{P}_{ind,1}$ and $\boldsymbol{P}_{ind,2}$ (the adjacent domains) is shown in figure 5. The angles between these vectors are determined as $\beta_{kl} = (\boldsymbol{P}_{ind,k}, \wedge \boldsymbol{P}_{ind,l}) = \cos^{-1}[\boldsymbol{P}_{ind,k} \cdot \boldsymbol{P}_{ind,l}/(|\boldsymbol{P}_{ind,k}||\boldsymbol{P}_{ind,l}|)]$. For example, independently of the unit cell parameters in the $3m$ phase, there is the angle

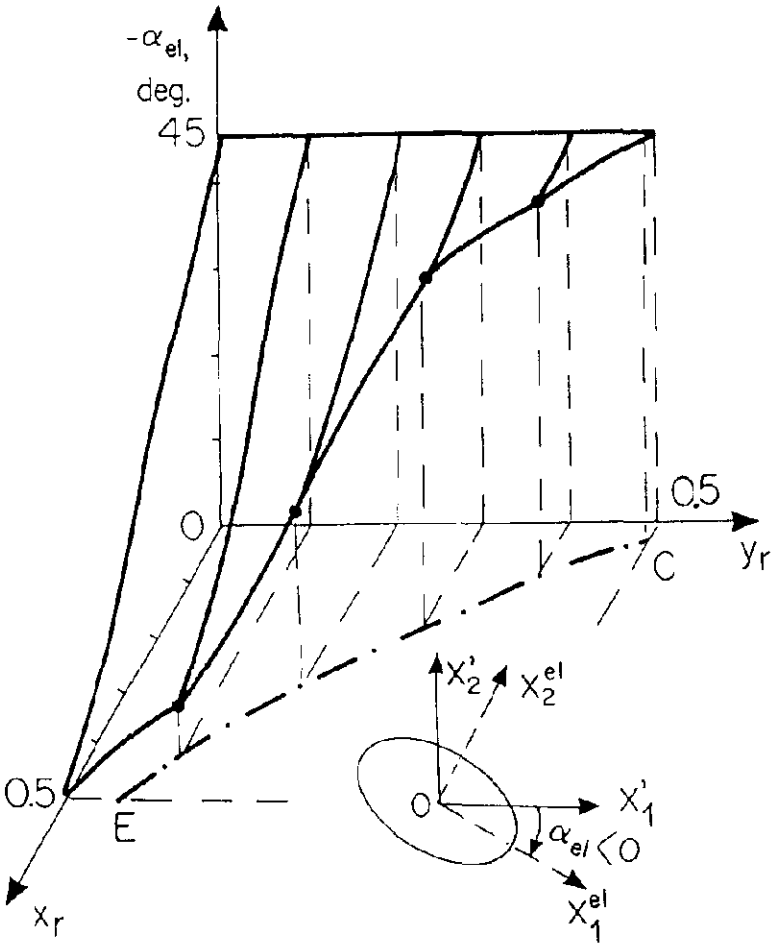

Figure 4. The dependence of the angle α_{el} $(x_r; y_r)$ according to equation (9), describing the rotation of the ellipse axes OX_i^{el} in the $(X_1'OX_2')$ plane (shown in the inset). The curve CE was taken from figure 3.

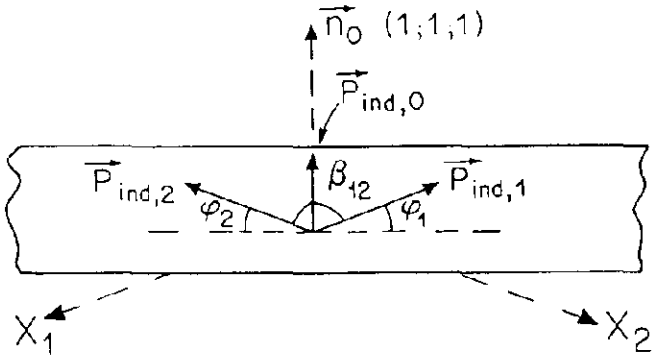

Figure 5. A scheme of the non-180° domain types with the induced polarization vectors $P_{ind,l}$ in the $3m$ phase of the $(111)_{cub}$ platelet of PMN crystals. n_0 (1; 1; 1) is the normal vector, $\beta_{12} = (P_{ind,1}; \wedge P_{ind,2}) = 109.47°$, φ_1 and φ_2 (= 35.26°) are the orientation angles.

$\beta_{12} = (P_{ind,1}, \wedge P_{ind,2}) \approx 109.47°$ between the inclined domains, which leads to the angles $\varphi_1 = \varphi_2 = (180° - \beta_{12})/2 \approx 35.26°$ between $P_{ind,1}$ and the $(111)_{cub}$ plane or between $P_{ind,2}$ and this plane.

To study the possibilities of elastic matching of the different domain types ($l = 0; 1; 2; 3$) we use their distortion matrices $\mathbf{N}_l$ from equations (2). The analysis of the conditions for the zero-net-strain plane at the domain boundary [10, 16, 22] shows the presence of such $\{100\}_{cub}$ planes between each two domain types, propagating in the platelike crystal.

An insertion of the third domain type results in excessive mechanical stress. Taking into account an interaction between the domains with $P_{ind,1}$ (volume concentration m) and $P_{ind,2}$ (volume concentration $1-m$) and the domain with $P_{ind,3}$ for example, we have the distortion matrices in the form of

$$\mathbf{M} = \begin{pmatrix} \eta_a & -\eta & \eta(1-2m) \\ -\eta & \eta_a & \eta(2m-1) \\ \eta(1-2m) & \eta(2m-1) & \eta_a \end{pmatrix} \qquad \mathbf{N} = \begin{pmatrix} \eta_a & \eta & -\eta \\ \eta & \eta_a & -\eta \\ -\eta & -\eta & \eta_a \end{pmatrix} \tag{10}$$

respectively. The invariants (5) containing the elements of equations (3) and (10) satisfy the conditions for the zero-net-strain planes if $m = 0$ or $m = 1$, i.e., the two domain types allowed by elastic matching only. This conclusion may also be correct for an interaction of the analogous 180° domain types (i.e., $P_{ind,1}$, $-P_{ind,1}$ and $P_{ind,3}$, $-P_{ind,3}$) which are allowed by the symmetry species $m\bar{3}m1'F3m1'$ [24] and have been experimentally evidenced during the electric field switching process under alternating polarity [5, 6].

Elastic matching of the four domain types in pairs (e.g. $P_{ind,0}$ and $P_{ind,1}$ with the volume concentrations k and $1-k$ as well as $P_{ind,2}$ and $P_{ind,3}$ with the volume concentrations l and $1-l$) gives a possibility for the realization of the zero-net-strain plane. The distortion matrices corresponding to these pairs

$$\mathbf{M} = \begin{pmatrix} \eta_a & \eta(2k-1) & \eta(2k-1) \\ \eta(2k-1) & \eta_a & \eta \\ \eta(2k-1) & \eta & \eta_a \end{pmatrix}$$
$$\mathbf{N} = \begin{pmatrix} \eta_a & \eta(1-2l) & \eta(2l-1) \\ \eta(1-2l) & \eta_a & -\eta \\ \eta(2l-1) & -\eta & \eta_a \end{pmatrix} \tag{11}$$

may be responsible for the zero-net-strain planes at the domain boundaries under favourable conditions resulting from analysis of equations (11), (3) and (5). Neglecting small terms proportional to η^4 we obtain the conditions

$$k + l = 1 \text{ or } k = 1. \tag{12}$$

Equations (12) may be interpreted as the conditions analogous to the ones for elastic matching of the four domain types (60° and 90°) in the orthorhombic phases of perovskite ferroelectric crystals [16, 22, 23] and may also be used for the description of 180° domain formation during the switching process in PMN. In particular the elastic behaviour of the domain types during the switching process within the temperature range of the induced polarization reversal and the possible violations of conditions (12) may have an influence on the features of the field-induced polarization P_{ind} of polydomain crystals and on a certain asymmetry of its temperature dependence $P_{ind}(T)$ (see e.g. figure 14 in [5]).

As a result, it should be noted that the interaction of the non-180° domains in the $3m$ phase of PMN is probably realized in ways analogous to those in other crystals undergoing the cubic–rhombohedral phase transition. This fact is associated with the symmetry of the unit cell and the domain structure in the rhombohedral phase as well as with the role of the internal mechanical stress accompanying the interaction of the non-180° domains.

5. Conclusions

The formation of polar macrodomain structure, various phase boundaries and the switching of the induced polarization related to the electric-field-induced first-order phase transition

from $m\bar{3}m$ to $3m$ in platelike PMN crystals have been analysed in the present work by crystallographic considerations and calculations on the basis of internal stresses and their relation to the unit cell parameters. The elastic interaction between the domains or phase regions and the mechanical stress has been shown to play an important role in the kinetics of this induced phase transition. A diagram describing the domain types and phase boundaries resulting from the $m\bar{3}m \leftrightarrows 3m$ phase transition has been proposed. This crystallographic analysis, based on the results of previous work [10, 14–18, 22, 23], was the first attempt at the interpretation of features of elastic interaction during the induced phase transition in a complex perovskite crystal. Some difficulties arose because of the limited experimental data on the mechanical properties of PMN single crystals. However, the results of our analysis have illustrated the good agreement with the macroscopic effects observed in PMN crystals and permitted us to substantiate the noticeable trends in complex behaviour of polydomain ferroelectric crystals within the phase transition region.

Acknowledgments

The authors are grateful to O Hirth and R Cros for technical help and to the Swiss National Science Foundation for partial support.

References

[1] Cross L E 1989 *Ferroelectrics* **90** 113
[2] Smolenskii G A 1970 *J. Phys. Soc. Japan* **28** (Supplement) 26
[3] Chen J, Chan H M and Harmer M P 1989 *J. Am. Ceram. Soc.* **72** 593
[4] de Mathan N, Husson E, Calvarin G, Gavarri J R, Hewat A W and Morell A 1991 *J. Phys.: Condens. Matter* **3** 8159
[5] Ye Z-G and Schmid H 1993 *Ferroelectrics* **145** 83
[6] Ye Z-G 1995 *Ferroelectrics* at press
[7] Lines M E and Glass A M 1977 *Principles and Application of Ferroelectrics and Related Materials* (Oxford: Clarendon)
[8] Roytburd A L 1993 *Phase Transitions* **45** 1
[9] Dunik E F and Shuvalov L A 1989 *Ferroelectrics* **98** 207
[10] Metrat G 1980 *Ferroelectrics* **26** 801
[11] Mendelson S 1981 *Ferroelectrics* **37** 519
[12] Chervonobrodov S P and Roytburd A L 1988 *Ferroelectrics* **93** 109
[13] Kuhn W J, Peterson J and Müser H E 1982 *Phys. Status Solidi* a **71** 483
[14] Balyunis L E, Topolov V Yu, Turik A V and Fesenko O E 1990 *Ferroelectrics* **111** 291
[15] Kuhn W J 1991 *Ferroelectr. Lett.* **13** 101
[16] Balyunis L E, Topolov V Yu, Ibrahima Sory Bah and Turik A V 1993 *J. Phys.: Condens. Matter* **5** 1419
[17] Topolov V Yu, Balyunis L E, Turik A V, Bah I S and Fesenko O E 1992 *Izv. RAN. Ser. Fiz.* **56** 127; 1992 *Bull. Acad. Sci. Russ. Phys. Ser.* **56** 1588
[18] Topolov V Yu, Rabe H and Schmid H 1993 *Ferroelectrics* **146** 113
[19] Korn G A and Korn T A 1968 *Mathematical Handbook for Scientists and Engineers* 2nd edn (New York: McGraw-Hill)
[20] de Mathan N, Husson E, Calvarin G and Morell A 1991 *Mater. Res. Bull.* **26** 1167
[21] Verbaere A, Piffard Y, Ye Z-G and Husson E 1992 *Mater. Res. Bull.* **27** 1227
[22] Topolov V Yu, Balyunis L E, Turik A V, Eremkin V V and Bah I S 1992 *Kristallografiya* **37** 433; 1992 *Sov. Phys.-Crystallogr.* **37** 223
[23] Gagarina E, Topolov V Yu, Tsikhotski E and Sakhnenko V 1992 *Ferroelectrics* **126** 335
[24] Aizu K 1970 *Phys. Rev.* B **2** 754